Case Studies in Thermal Engineering 37 (2022) 102262

Contents lists available at ScienceDirect

Case Studies in Thermal Engineering

journal homepage: www.elsevier.com/locate/csite

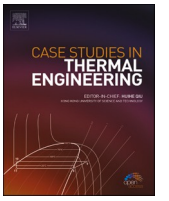

Study on improving the storage efficiency of ocean thermal energy storage (OTES) unit by using fins

Shizhen Li [a], Yulong Zhang [a], Zhengtong Zhou [a], Wenzhuo Shi [a,*], Jingzhi Zhang [b], Bingzhen Wang [c]

[a] Institute of Marine Science and Technology, Shandong University, Qingdao, PR China
[b] School of Energy and Power Engineering, Shandong University, Jinan, PR China
[c] National Ocean Technology Center, Tianjin, PR China

ARTICLE INFO

Keywords:
Ocean thermal energy storage
Phase change material
Fractal fins
Liquid phase rate
Solidification performance

ABSTRACT

It is a central challenge for energy self-supplied underwater vehicles converting the huge ocean thermal energy to electrical energy effectively. However, the energy storage efficiency of ocean thermal energy storage (OTES) unit limits the conversion efficiency. Fins are proposed for OTES unit to improve energy storage efficiency in this paper. Firstly, this paper develops a non-stationary model of solidification heat transfer for OTES unit and uses FLUENT to accomplish its numerical analysis. Then, the influence of radial fin and fractal fin on the solidification behavior of phase change material (PCM) are compared. Finally, several fractal fins with different fractal levels, bifurcation angles and ambient temperature are analyzed for the evolution of the liquid phase rate and temperature distribution of PCM. The results show that fractal fins can reduce the solidification time of PCM by 34.46% compared with radial fins. Furthermore, the solidification rate of PCM can be improved by increasing the number of fractal levels and choosing a proper bifurcation angle. However, the solidification behavior of PCM changes slightly when the fractal level increases to 3. The bifurcation angle of 90° is appropriate for practical applications. Furthermore, keeping the temperature difference above 10K can achieve faster solidification.

Nomenclature

c_p	Specific heat
g	Liquid phase ratio
H/h	Enthalpy
k	Thermal conductivity
L	Latent heat
l_n	Length of fins
N	Scale factor of the fins
r	Polar diameter
r_i	Inner radius of inner tube

* Corresponding author.
E-mail address: wzshi@sdu.edu.cn (W. Shi).

https://doi.org/10.1016/j.csite.2022.102262
Received 4 May 2022; Received in revised form 17 June 2022; Accepted 1 July 2022
Available online 14 July 2022

r_o	outer radius of inner tube
R_i	Inner radius of outer shell
R_o	outer radius of outer shell
R_c	Coupled heat exchange boundary
T_{ref}	Initial reference temperature
T_s	Solidification temperature
T_l	Melting temperature
T_f	Fin temperature
T_p	Phase change material temperature
T_w	Heat exchanger tube wall surface temperature
ν	Kinematic viscosity
w_n	Width of fins

Greek Alphabets

α	Bifurcation angle
β	Coefficient of thermal expansion
ρ	Density
τ	Polar angle

Subscripts

c	coupling
f	metal fins
i	inner
l	liquid
n	fractal level
o	outer
p	phase change material
s	solid
w	wall
mush	mushy zone
ref	initial reference state

Abbreviations

OTES	Ocean Thermal Energy Storage
PCM	Phase Change Material

1. Introduction

The ocean cover 71% of the earth's surface and contain abundant resources. Consequently, it is crucial for the sustainable development of humanity to explore and develop ocean resources [1,2]. Ocean observation and development are inseparable from underwater vehicles, such as buoys. Underwater vehicles are normally powered by batteries with a certain capacity, which limits their

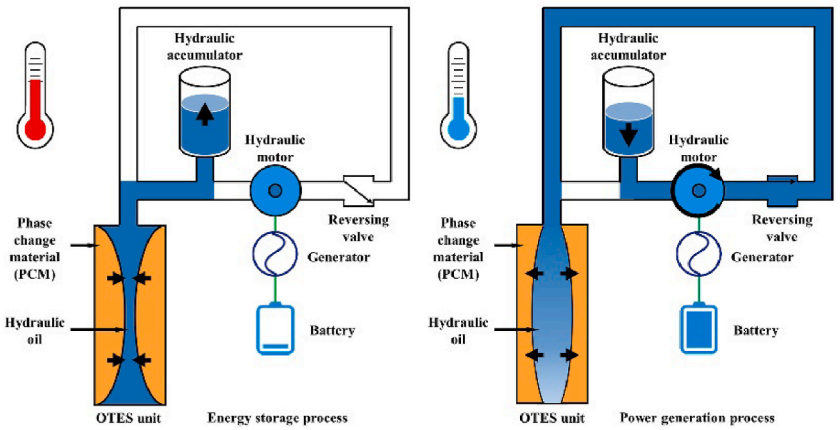

Fig. 1. Ocean thermal power generation system based on solid-liquid phase transition.

autonomy and working time [3,4]. As buoy operations become increasingly difficult, energy supply becomes a bottleneck limiting deep-water observation and operation [5]. Many scholars solve this problem by using an ocean thermal energy conversion technology, which based on solid-liquid phase transformation [6,7]. This technology's operating principle is illustrated in Fig. 1. This technology can cause the volume change of PCM in OTES unit by using temperature difference between ocean surface and deep sea [8]. The ocean heat captured in this process can be stored by an electromechanical system [9,10], where the OTES unit is the most significant unit, and its storage efficiency affects the energy supply of the entire equipment. Among them, Webb [11] et al. applied ocean thermal energy conversion technology to SLOCUM and transformed SLOCUM into an underwater thermal glider. NASA's Jet Propulsion Laboratory has joined forces with several units to develop a new unmanned submersible powered by ocean thermal energy, which can replenish its batteries with roughly 1.6 $W \cdot h$ of energy in a single section movement [12].

The PCM used in the OTES unit, such as paraffin, which has a higher latent heat of phase change and thermal expansion rate typically. On the other hand, PCM has a low thermal conductivity. Pure liquid PCM has a substantially lower thermal conductivity than pure solid PCM, which resulting long phase change time of PCM and the low energy storage efficiency of OTES unit. It can be observed that reducing the solidification/melting time of PCM is the key to enhance the storage efficiency of OTES unit. Currently, there are two main methods to quicken the slow heat transfer rate of the PCM phase change. One is using composites of pure paraffin mixed with high thermal conductivity materials as the working medium, such as foam metal, graphite mixed with paraffin [13,14], and the other is to add thermal conduction structures for the energy storage units, like fins [15,16].

The structure, size, and distribution type of the fins all have an impact on the PCM's heat transfer performance. As a result, optimizing the fin structure, size, and other factors has become critical to enhance the OTES unit's energy storage efficiency. Abdu Lateef et al. [17] has summarized the application status of embedding fins onto PCM in previous study. They investigated the effect of fin shape and dimensionless number on the heat transfer properties of PCM and concluded that the radial fin structure is the most effective way to improve PCM heat transfer. Tay et al. [18] used Computational Fluid Dynamics (CFD) technology to compare and analyze the impact of the needle structure and the fin structure on the solidification process of the phase change thermal energy storage system, and discovered that the fin structure was more beneficial to PCM solidification than the needle structure. Juan Duan et al. [19] evaluated the heat transfer enhancement effectiveness of many spiral fins and longitudinal fins, and indicated that spiral fins solidify 74.13% faster than longitudinal fins. Rozenfeld et al. [20] used spiral fins in a thermal energy storage unit, performed mathematical modeling for the unit, and tested the model's correctness. Al-Abidi et al. [21,22] considered the number, length, and thickness of the fins, and studied the influence of internal fins on the solidification process in the heat exchanger. Hosseini et al. [23] investigated the solidification of a latent heat storage system with longitudinal fins, pointing out the influence of fin height and the number of stefan on PCM solidification. Their results revealed that raising the fin height could significantly reduce solidification time. Increasing the number of stefan, on the other hand, accelerates the vortex generating speed induced by the fins. Zhao, M et al. [24] used numerical simulation methods to optimize the topology of the radial fins. The results showed that the model after topology optimization had a 70% reduction in heat storage time and an 81% reduction in heat release time compared with the model before optimization. Sciacovelli et al. [25] innovatively proposed tree-shaped fins for the PCM latent heat storage system and optimized the shape of the tree-shaped fins. The system was evaluated by using the CFD model and response surface method. Moreover, the results showed that the storage efficiency of the optimized system increased by 24%. Zhang, C et al. [26] designed a latent heat storage unit based on the fractal theory, studied the transient temperature distribution and the evolution of the solid-liquid interface, and proposed an appropriate length ratio and width index for the fin structure.

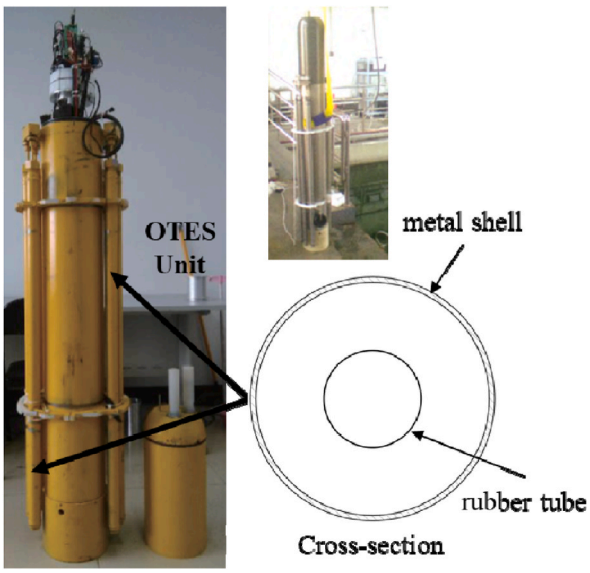

Fig. 2. Prototype of underwater vehicle and energy storage unit of previous work.

According to the existing surveys, altering the kind of fin structure and adjusting the fin size can assist to enhance the PCM's heat transfer rate. However, the related research had never been done in the field of ocean thermal energy conversion. In addition, only the finless shell-and-tube structure was applied as the OTES unit in the underwater vehicle with experiments in Wang et al.'s work [27]. The prototype of underwater vehicle and the energy storage unit used in the experiment are shown in Fig. 2. The underwater vehicle's navigation speed will be reduced when throughout the ocean thermal energy conversion phase, which ensuring the full conversion of ocean thermal energy in practical applications. However, it was found that the finless shell-and-tube OTES unit had a negative impact on the energy conversion efficiency of the whole device in the experiment. Furthermore, the sample time of an underwater vehicle outfitted with OTES unit was significantly longer than that of a standard underwater vehicle, which would reduce the underwater vehicle's efficiency drastically. As a result, the fins are added to the OTES unit in this paper, and *n*-hexadecane is used as PCM to study the solidification process. Five different fin models are built, and the solidification of PCM in fin-enhanced OTES unit is investigated by using a combination of numerical simulation and FLUENT software. The authors concentrate on the impacts of the fractal level, bifurcation angle and the ambient temperature on the OTES unit's energy storage efficiency.

2. Physical model and numerical methods

2.1. Description of the OTES unit

The OTES unit includes a shell and tube heat exchanger, which consists of a metal outer shell and a rubber inner tube. The PCM is *n*-hexadecane, which is placed in the cavity between the outer shell and the inner tube. Hydraulic oil is stored in the inner tube as the working medium of the electromechanical system. The solidification heat transfer performance of five models are studied in this paper under the condition that a specific PCM mass is guaranteed. Moreover, the volume ratio in the model with fins is around 10%. Because OTES unit is vertically positioned in the water, the vertical change trend of each cross-section is assumed the same [21,28]. The detailed parameters of the metal, rubber and PCM are shown in Table 1.

The physical models studied in this paper are shown in Fig. 3. Model-1 has no fins; Model-2 has four radial fins; Model-3 has 1-level fractal fins; Model-4 has 2-level fractal fins; and Model-5 has 3-level fractal fins. The computational domain is a ring-shaped closed zone where the PCM is stored. The detailed fin structure displays the fractal fin geometry parameters.

The outer shells and inner tubes of the above five models have the same dimensions and materials. Among them, the material of inner tubes is Nitrile rubber, while the outer shells and the fins are manufactured by 3D printing technology with the material of Aluminum alloy. The inner tube has an inner radius r_i of 17 mm and an outer radius r_o of 15 mm. As well as the inner radius R_i and the outer radius R_o of the outer shell is 50 mm and 60 mm separately. The initial value of the bifurcation angle α for each level is 90°.The dimensions of the fins models obtained by equation (1).

$$l_{n+1}/l_n = w_{n+1}/w_n = N \tag{1}$$

where l_n is the length of the n-level fins; w_n is the width of the n-level fins; N is the scale factor of the fins with an initial value of $\sqrt{2}/2$. Other dimensional parameters are shown in Table 2.

2.2. Mathematical modeling and numerical approach

The purpose of the study is to investigate the influence of fin types and corresponding configurations on the solidification heat transfer performance of PCM in the OTES unit. Furthermore, the literature [26] has demonstrated that the solidification process of PCM is an unstable heat conduction problem, where the heat transfer exists not only between the shells and the fins but also between the fins and the PCM. The following assumptions are adopted to simplify the heat transfer model with an unstable heat release process:

(1) Within an OTES unit, PCM can appear in three states: solid state, liquid state, and solid-liquid two-phase mushy zone [26];
(2) The laminar flow model is used to solve the phase change process of PCM, which is a low velocity unsteady and incompressible flow process;
(3) Ignore the influence of natural convection on the solidification process, because the flow velocity caused by the density difference between different phases of PCM is very small;
(4) Ignore the heat transfer resistance of the heat exchange tube wall, because there is almost no heat loss on the heat exchange tube wall in actual engineering.

Based on physical models, a two-dimensional transient heat transfer model is proposed as shown in Fig. 3, using the enthalpy

Table 1
Thermo-physical properties of *N*-hexadecane [29], Aluminum alloy and Nitrile rubber.

Parameter	Unit	*N*-hexadecane	Aluminum alloy	Nitrile rubber
Density [ρ_s/ ρ_l]	kg/m^3	864/776.3	2703	999
Specific heat [c_{ps}/ c_{pl}]	$kJ/(kg\cdot K)$	1.64/2.09	0.963	1.97
Thermal conductivity [k_s/ k_l]	$w/(m\cdot K)$	0.313/0.140	180	0.25
Latent heat [L]	J/kg	236000	–	–
Melting temperature [T_s/T_l]	K	289.15/291.15	–	–
Kinematic viscosity [ν]	m^2/s	4.46×10^{-6}	–	–
Volume expansion coefficient [β]	$1/K$	0.89×10^{-3}	–	–

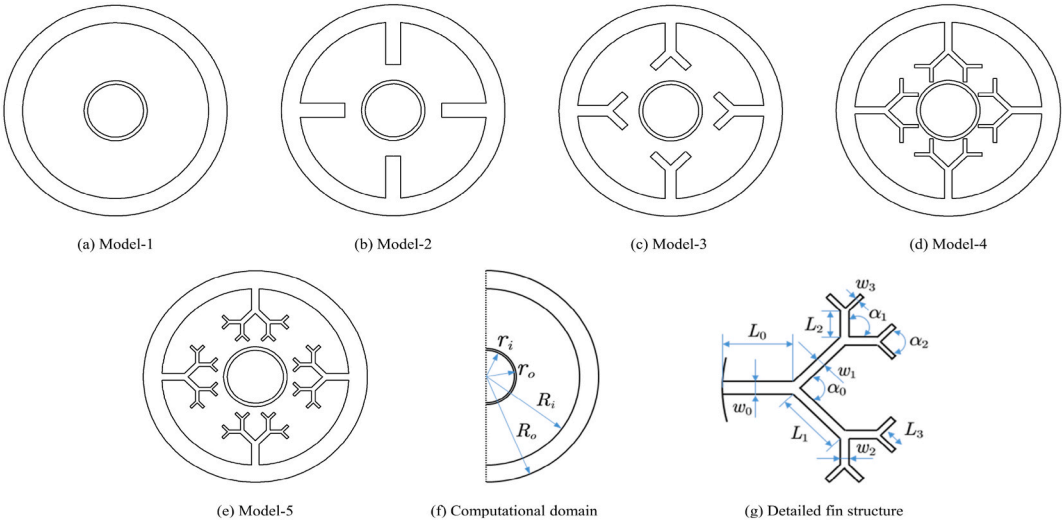

Fig. 3. Physical models for the present study: (a) the model without fins; (b) the model with radial fins; (c) the model with 1-level fractal fins; (d) the model with 2-level fractal fins; (e) the model with 3-level fractal fins; (f) computational domain of the OTES unit; (g) detailed explanation of fractal fin structure parameters.

Table 2
Physical model parameters.

Parameter	l_0/mm	l_1/mm	l_2/mm	l_3/mm	w_0/mm	w_1/mm	w_2/mm	w_3/mm
Model-2	12.00	–	–	–	4.00	–	–	–
Model-3	8.00	5.66	–	–	3.00	2.12	–	–
Model-4	8.00	5.66	4.00	–	2.00	1.40	0.98	–
Model-5	6.00	4.20	3.00	2.10	2.00	1.40	0.98	0.71

method, which is often utilized to calculate the solidification/melting process. This method takes the temperature and enthalpy of the PCM as solution variables, unifies the entire zone (including the solid phase zone, liquid phase zone, and two-phase mushy zone), establishes an energy equation to find the enthalpy distribution, and calculates the node temperature based on the relationship between enthalpy and temperature. The following is the unified energy equation:

$$\partial(\rho H)/\partial t = k\left[\partial^2 T/\partial r^2 + 1\cdot\left(\partial^2 T/\partial \tau^2\right)/r^2\right] \tag{2}$$

where H represents the total enthalpy per unit volume of the PCM; ρ, k represents the material density and thermal conductivity, r andτ represent the polar diameter and the polar angle in cylindrical coordinates respectively.

The enthalpy of the solid phase zone, liquid phase zone, and mushy zone are different for the PCM. The enthalpy of the solid phase zone and the mushy zone only contains sensible heat h, but the enthalpy of the liquid phase zone and the mushy zone has both sensible and latent heat ∇h. The following are the equations for the enthalpy of the solid and liquid phase:

$$h_s = \int_{T_{ref}}^{T} c_{ps}dT \tag{3}$$

$$h_{mush} = \int_{T_l}^{T_s} c_{pmush}dT + \nabla h_{mush} \tag{4}$$

$$h_l = \int_{T_l}^{T} c_{pl}dT + \nabla h_l \tag{5}$$

where h_s, h_{mush}, h_l, c_{ps}, c_{pmush} andc_{pl} represent the enthalpy and specific heat capacity of the solid phase zone, liquid phase zone, and mushy zone respectively.T_{ref}, T_s andT_l represent the initial reference temperature, PCM solidification temperature, and PCM melting temperature respectively.

The liquid phase ratio g is introduced to express the volume ratio of the PCM in the mushy zone, where$g$ is defined as:

$$g = \begin{cases} 0 & T < T_s \\ (T - T_s)/(T_l - T_s) & T_s \leqslant T < T_l \\ 1 & T \geqslant T_l \end{cases} \tag{6}$$

Given the liquid phase ratio, the enthalpy expression can be unified into an equation as the following:

$$h = \int_{T_{ref}}^{T} c_p dT + g \cdot \nabla h \tag{7}$$

2.3. Boundary conditions and initial conditions

The outer wall of the OTES unit is in touch with seawater, which is applied as the heat exchange fluid. Specifically, the heat exchange fluid performs convective heat exchange with the outer wall in theory, and then the temperature in the inner wall will be greater than that in the outer wall. The heat flux in the seawater is transferred in the radial direction of the OTES unit from the outer wall surface to the inner wall surface. The heat transfer resistance is overlooked in this study due to the thinness of the heat transfer wall; therefore, the outside wall is simplified to a constant temperature condition as follows:

$$r = R_o; \quad T|_{r=R_o} = T_w \tag{8}$$

where T_w represents the temperature of the outer wall.

The inner wall surface of the OTES element is approximated as an adiabatic boundary in order to simplify the model, which described by the following equation.

$$(\partial T/\partial r)|_{r=R_i} = 0 \tag{9}$$

The solid-liquid interface has a coupled heat transfer boundary that ensures temperature and heat flow continuity, which has the following mathematical expression:

$$T_s|_{r=R_c} = T_l|_{r=R_c} \tag{10}$$

$$-k_s(\partial T_s/\partial r)|_{r=R_c} = -k_l(\partial T_l/\partial r)|_{r=R_c} \tag{11}$$

where k_s andk_l represent the thermal conductivity of the PCM solid phase zone and liquid phase zone respectively. R_c represents the coupled heat transfer boundary.

The contact surface between the fins and the phase change material is also coupled heat transfer boundary. It has the following mathematical expression:

$$T_f\big|_{r=R_c} = T_p\big|_{r=R_c} \tag{12}$$

$$-k_f\left(\partial T_f/\partial r\right)\big|_{r=R_c} = -k_p\left(\partial T_p/\partial r\right)\big|_{r=R_c} \tag{13}$$

where T_f, T_p, k_f, k_p represent the temperature and thermal conductivity of the coupling boundary between the fin and PCM.

The fin and PCM reach thermal equilibrium at the initial moment. In addition, the temperature in the entire calculation domain remains unchanged, which has the following mathematical expression:

$$T(r,\tau,T)|_{r=0} = T_{ref} \tag{14}$$

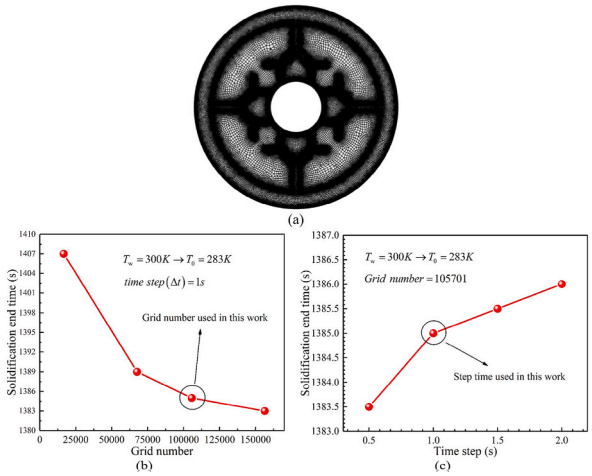

Fig. 4. Independence verifications: (a) model meshing; (c) grid number comparison analysis; (b) time step comparison analysis.

3. Numerical verification and validation

3.1. Independence validations of grid and step time

Based on the enthalpy method, this paper solves the phase change process for the OTES unit by using the transient solidification/melting model, which in the FLUENT2021 software. The calculation method uses SIMPLE pressure-velocity coupling algorithm and coupled heat transfer to solve the energy equation. The convection term of the energy equation is discretized using a second-order upwind scheme, and the under-relaxation factors of density, pressure and momentum are 1.0, 0.2 and 0.9 respectively.

The changes in the solidification end time of PCM are compared under the conditions of four grid numbers and four step time to verify the independence of the numerical calculation method. As presented in Fig. 4(a), a quadrilateral mesh is used to partition the model. The grid consists of two zones: one is the thermally conductive metal zone, which is divided by a fine grid because of the large temperature gradient in this zone; the other is the zone composed of PCM, which is divided by a coarse grid. The number of grids and time steps of the OTES unit with fractal fins (Model-4) are independently validated.

Firstly, the grid configurations are independently verified by setting the grid sizes to 0.1 mm, 0.5 mm, 1 mm and 2 mm in succession, while 156359, 105701, 67637 and 16634 are the matching numbers of grids. The time step keeps at 1s in this period. Fig. 4(b) reflects the solidification end time varying with the grid number. When the number of grids is larger than 60000, the result reveals that the inaccuracy keeps within 0.28%. Therefore, the accuracy of the data can be guaranteed if the number of grids exceeds 60000 in this case. Considering the operating conditions of the computer, the grid number 105701 is used here. Then the grid is divided into cells with a cell size of 0.5 mm to search the effect of different time steps. Four different time steps (0.5s, 1.0s, 1.5s and 2.0s) are selected in this study. As demonstrated in Fig. 4(c), when the time step lager than 1s, the solidification end time changes negligible. In order to save time, 1s is chosen as the time step for the numerical simulation.

3.2. Model verification

The simulation results are compared with available experimental data from Ismail et al. [28] in order to assess the feasibility of the methods used in this paper. In the simulation, the same parameters and boundary conditions as in the literature are utilized, and the PCM's starting temperature is 338.15K. The metal inner tube's inner wall is kept at a constant temperature. Fig. 5 represents the comparison graphs of the existing method and present method. The curves in this figure show the position of the PCM phase transition intersection at different times (30min, 60min and 90min). According to Fig. 5, it can be seen that the maximum error between the experimental results and the simulation results is less than 5%. Considering the heat loss reported in the literature, the simulation method used in this study is better and feasible.

4. Results and discussion

4.1. Analysis of solidification energy storage process

The evolution of the PCM liquid phase rate (left part) and average temperature distribution (right part) of Model-1, Model-2 and Model-3 in OTES unit are shown in Table 3. It is clear that the liquid phase change speed of the OTES unit with fins is much faster than that of the OTES unit without fins by comparing the liquid phase rate cloud diagrams of Model-1, Model-2 and Model-3. This indicates that the fin help to improve the energy storage efficiency of the OTES unit apparently. The liquid phase rate of PCM in the OTES unit is directly related to the geometry of the fins by comparing the liquid phase rate cloud diagrams of Model-2 and Model-3. Specifically, Model-2 and Model-3 here have the same solid volume but different fin types and configurations. During the early stage of solidification, high thermal conductivity metal such as metal shells and fins directly contact and transfer heat with the PCM, and the liquid phase of the PCM shrinks continuously around the geometric contours of the shell and the fins. As time goes by, the thickness of the PCM solid layer around the shell and the fins increases. The PCM mostly relies on heat transfer between the solid and liquid layers at

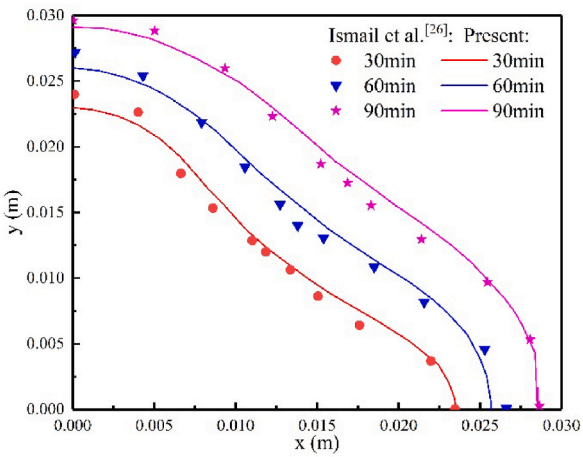

Fig. 5. Validation of the feasibility of present research methods.

Table 3
Evolution of liquid phase rate and temperature distribution of OTES unit with different fins.

t/s	Model-1	Model-2	Model-3		Model-1	Model-2	Model-3	
	Liquid fraction				Temperature distribution			
60				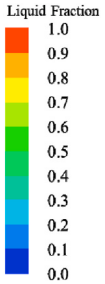	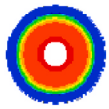			
300					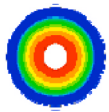			
900					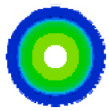			
1500			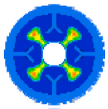		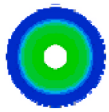			
2100					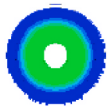		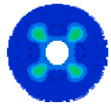	

this stage, with the liquid layer's heat being released through the solid layer and high thermal conductivity metal. The heat exchange rate between the high thermal conductivity metal and the PCM decreases due to the PCM's low thermal conductivity. In addition, the cloud diagrams show that the liquid areas of PCM in Model-2 and Model-3 are nearly the same in the early stages of solidification ($t < 300s$). It demonstrates that the similar effects of radial fins and fractal fins on PCM solidification behavior in the early stage. However, liquid area reduction in Model-3 is substantially higher than that in Model-2, which is apparent in the late solidification stage (900s–2100s). At 2100s, the PCM of Model-3 is almost completely solid, while nearly 15% of the PCM in Model-2 is liquid. Compared with the radial fin, the fractal fin have a better positive influence on the solidification behavior of PCM.

The temperature distribution of PCM is shown on the right side of Table 3. The shape of the temperature distribution is similar to the shape of the liquid phase rate evolution. The temperature gradient of Model-1 is smaller at each step than that of Model-2 and Model-3 due to its finless condition, which demonstrates the importance of fins in accelerating the solidification behavior of PCM. Due to the different inner structures in Model-2 and Model-3, they have different actual heat transfer areas despite the same solid volume. The fractal fins in Model-3 are more ductile than the radial fins in Model-2, which allows the fins to extend into the PCM. Further, it allows the heat from the liquid PCM around the rubber inner tube to be quickly transferred through the fins, and the heat is transferred to the metal shell, which speeds up the solidification process.

The variation trends of liquid phase rate and solidification end time resulting from the three models are shown in Fig. 6. The PCM in Model-3 has completed solidification behavior at 2330 s, while 44% and 11% of the PCM in Model-1 and Mode-2 have not yet solidified respectively, which is represented in Fig. 6(a). The solidification behavior of each model is quantitatively assessed and compared in Fig. 6(b). In detail, the solidification end times of the three models are 9417s, 3514s and 2330s, respectively. The solidification end time of Model-2 and Model-3 are significantly shorter than that of Model-1 by 62.69% and 75.26%. Furthermore,

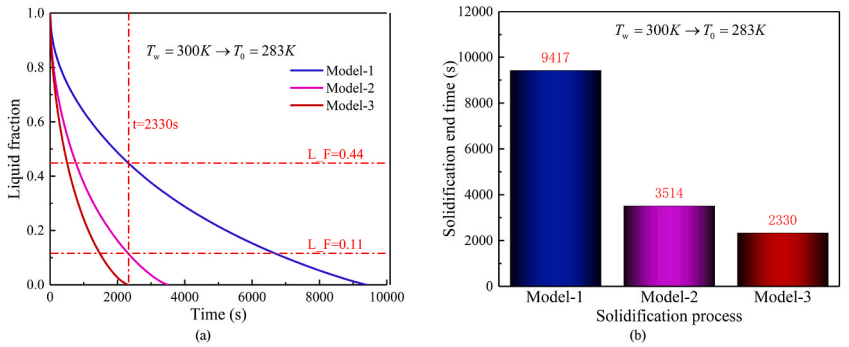

Fig. 6. Effect of fin structure type on solidification behavior: (a) computed variation of liquid fration with time; (b) solidification end time comparison.

Model-3 reduces the solidification end time by 34.46% than Model-2. Consequently, the fractal fins in Model-3 have better heat transfer performance than the radial fins in Model-2, and the adding of fractal fins can significantly increase the OTES unit's energy storage efficiency. Therefore, the following will emphasize on fractal fins' extended structure of Model-3.

4.2. Effect of structure type, geometric parameters and environmental conditions

Fractal levels, fin size parameters (length and width), and bifurcation angle of fractal fins all play important roles in the solidification performance of PCM. Fractal levels, bifurcation angle and deep-sea temperature are discussed in this section independently.

4.2.1. Effect of the fractal levels

It's worth noting that the dimensional parameters (length and width) of the fractal fins decreases as the fractal fin levels increases, while the solid volume of the fractal fin remains constant. The cloud diagrams of PCM liquid phase rate for three fractal levels (F_L = 1, 2, 3) are presented on the left side of Table 4. In detail, the liquid phase zones of the three models are nearly identical at 60s, demonstrating that the fractal levels of the fins have little impact on the PCM's liquid phase rate evolution in the early stages. However, in the time range of 300–1200s, the liquid phase rate of the three models have a significant variation, that is, as the number of fractal levels increases, the liquid phase zone of PCM shrinks faster. This phenomenon means that the PCM solidifies faster during this time period. And the reason is that the structure of the fractal fins spreads further to the edge of the rubber inner tube as the fractal levels increases. This enables the PCM to directly contact the high thermal conductivity metal fins near the rubber tube's inner wall and quickly transfer its own heat through the fins.

The temperature distribution of PCM is visibly affected by fractal levels, which is shown on the right side of Table 4. In addition, the PCM contains a two-phase coexistence zone (the mushy zone) during the phase change process. The latent heat of phase change is gradually released in this zone, and the solid-liquid boundary advances from the outside to the inside. Because the PCM with low thermal conductivity is regarded as equivalent thermal resistance here, the heat exchange rate from the rubber inner tube to the metal shell slows down due to the equivalent thermal resistance becoming larger, which is most significant in the pre-solidification and post-solidification periods., Therefore, the temperature changing in the mid-solidification period is negligible (around 300s). Furthermore, the fractal levels' effect on the temperature distribution of PCM is particularly apparent in the post-solidification period (900–1200s). The reason for this phenomenon is that a certain volume of PCM is divided into more small zones by the fractal fins as the number of fractal levels increases. Consequently, surrounded by more fins, the equivalent thermal resistance becomes smaller, thus the corresponding solidification behavior is optimized.

The variation trends of liquid phase rate with different fractal levels is shown in Fig. 7(a). The solidification end time of PCM decreases as the number of fractal levels increases, which is consistent with the results shown in Table 4. The fractal levels and the solidification rate of PCM are not positively correlated in the early stages ($t < 400s$), and the PCM for the Model-3 solidifies faster than that for the Model-4 and Model-5 until 220s. The reason for this phenomenon is that the heat capacity, the length and width of the fins in Model-3 are greater than that of Model-4 and Model-5. As demonstrated in Fig. 7(b), the solidification end time for the Model-4 and Model-5 are significantly shorter than that of Model-3 by 35.32% and 41%. Furthermore, the 3-level fins reduce the solidification end time by 8.79% than the 2-level fins. Therefore, the solidification rate of PCM increases with the number of fractal fin levels, and thus the energy storage efficiency of OTES unit can be improved.

4.2.2. Effect of the bifurcation angle

In this section, the solidification behavior effect of bifurcation angle on the PCM is further explored. Five fin structures are created

Table 4
Evolution of liquid phase rate and temperature distribution of the OTES unit with different fractal levels.

t/s	F_L = 1	F_L = 2	F_L = 3	F_L = 1	F_L = 2	F_L = 3
	Liquid fraction			Temperature distribution		
60						
300						
900						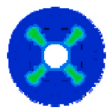
1200					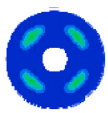	

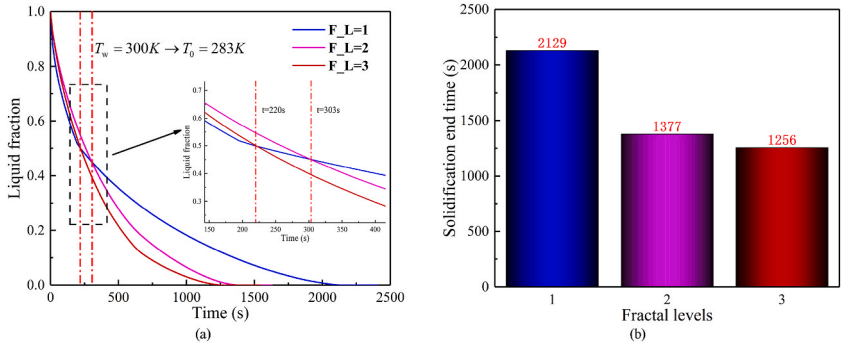

Fig. 7. Effect of fin fractal levels on solidification behavior: (a) computed variation of liquid fration with time; (b) solidification end time comparison.

with varied bifurcation angles, while the bifurcation angles, the material parameters, the dimensional parameters and the solid volume of each fin levels are the same, as shown in Fig. 8.

The evolution of liquid phase rate for different bifurcation angle is shown in Fig. 9(a). The solidification rate of the five models are nearly identical at the early stages of solidification, so it can be considered that bifurcation angle has little effect on the solidification behavior here. As time goes by, the solidification rate of the PCM steadily reduces as the bifurcation angle grows with fixed step size. The reason for this phenomenon is that the fractal fins gradually expand to the metal shell as the bifurcation angle grows, while the topmost fins gradually move away from the rubber inner tube. In addition, because the PCM near the rubber inner tube is separated from the fins by a rather thick layer of liquid PCM, which has a lower heat conductivity than solid PCM, the PCM near the metal shell dissipate heat more easily than that near the rubber inner tube. Consequently, the average solidification rate of PCM become smaller as a whole. The solidification end time for different bifurcation angles is illustrated in Fig. 9(b). The bifurcation angles are set to 90°, 105°, 120°, 135° and 150°in succession, while the PCM solidification end time is 1256s, 1325s, 1450s, 1523s and 1805s, respectively. Specifically, the growth rate of the PCM solidification end time are 5.49%, 9.43%, 5.03% and 18.52% as the angle gradually increases in step of 15°. Furthermore, the growth rate of PCM solidification end time are all below 10% until the bifurcation angle reaches 135°. However, the PCM solidification end time increases dramatically as the bifurcation angle exceeds 135°. Consequently, the OTES unit's energy storage efficiency has a negative correlation with the bifurcation angle, which is most significant when the angle exceeds 135°.

4.2.3. Effect of the deep seawater temperature

Because Model-5 has the best performance to improve the storage efficiency of OTES unit than other models in the previous analysis m, the evolution of the liquid phase rate for Model-5 under different water temperature is shown in Fig. 10(a). In particular, the solidification rate of PCM decreases progressively and the solidification end time increases gradually with the water temperature rising. This phenomenon is caused by the difference reduction between water temperature and PCM solidification temperature as the water temperature rises, while the solidification temperature of PCM is fixed. Therefore, a large temperature difference between seawater and PCM solidification temperature can achieve better thermal drive capability and faster PCM solidification rate. In addition, the solidification end time of PCM under three different temperature conditions is 907s, 1256s and 2113s respectively, as shown in Fig. 10(b). In addition, the increase rate of solidification end time between 280K and 283K, 283K and 286K are 38.48% and 68.23% respectively. Consequently, a considerable temperature difference is required to optimize the OTES unit's energy storage efficiency, which is chosen as 10K in operation.

5. Conclusions

The application of fins is proposed in this paper to improve the energy storage efficiency of OTES unit. Moreover, the effects of finless, radial fins and fractal fins for PCM are compared on the energy storage efficiency of OTES unit. Additionally, fractal fins with different fractal levels, multiple bifurcation angles and various seawater temperature conditions are researched further.

The fin structure can reduce the time needed for PCM to solidify, thus increase the OTES unit's energy storage efficiency. Specifically, with the same volume ratio of the fins, the fractal fins reduce the solidification end time by 75.26% and 34.46% than the finless structure and the radial fins respectively, which have the best heat transfer performance.

As the number of fractal levels grows, the solidification time of PCM decreases dramatically. The solidification end time is reduced by 35.32%, 41% and 8.79% respectively, when compared to the previous level of the model. Because fractal fins with more than 3-level fins are difficult to achieve for manufacture limitations, 3-level fractal fins are chosen for practical applications in this study. Besides, the growth rate of the solidification end time of the phase change material were 5.49%, 9.43%, 5.03% and 18.52% when the bifurcation angle is gradually increased in steps of 15°. The fractal angels have a negative correlation with the OTES unit's energy storage efficiency, which is most significant when the angle exceeds 135°', thus 90° is suggested for practical applications. The difference between seawater temperature and PCM solidification temperature has a positive correlation with the OTES unit's energy storage efficiency, and the increase in solidification end time between 280K and 283K, 283K and 286K was 38.48% and 68.23%.

In practical applications, OTES units use 3-level fractal fins with a fractal angle of 90° and keep the temperature difference above 10K, which will reach the better energy storage efficiency.

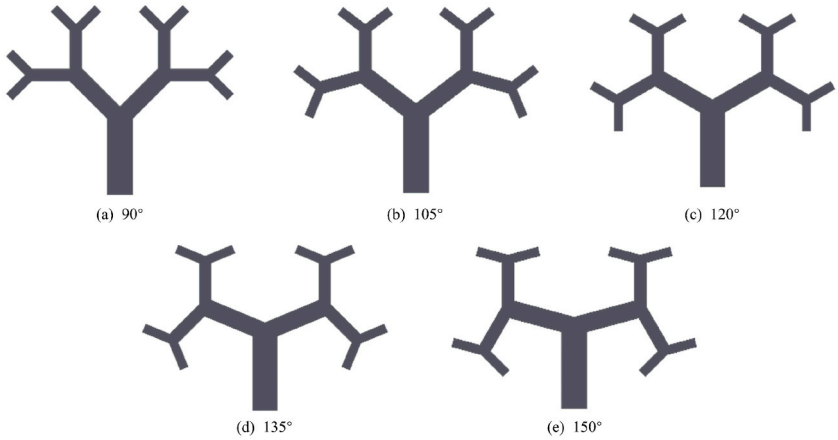

Fig. 8. Model diagrams of different bifurcation angles:(a)$\alpha = 90°$; (b)$\alpha = 105°$; (c)$\alpha = 120°$; (d)$\alpha = 135°$; (e)$\alpha = 150°$.

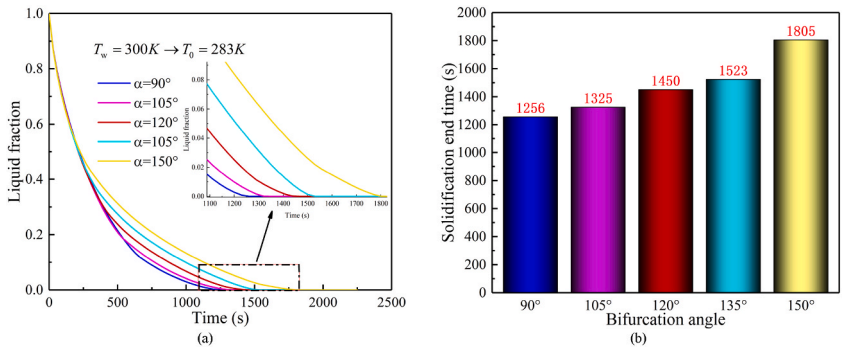

Fig. 9. Effect of fin bifurcation angle on solidification behavior: (a) computed variation of liquid fration with time; (b) solidification end time comparison.

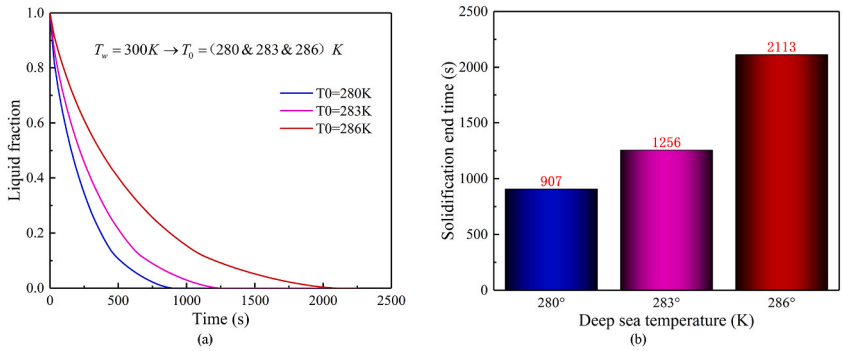

Fig. 10. Effect of deep seawater temperature on solidification behavior: (a) computed variation of liquid fration with time; (b) solidification end time comparison.

Author statement

The first author: Conceptualization, Funding Acquisition, Data analysis, Writing - Original Draft, Supervision, Project Administration.

The second author: Investigation, Methodology, Writing - Original Draft, Data analysis, Resources.

The third author: Investigation, Data analysis.

The fourth author (Corresponding author): Writing - Review & Editing, Validation, Project Administration.

The fifth author: Methodology, Research method guidance.

The sixth author: Writing - Review & Editing.

Declaration of competing interest

The authors declare that they have no known competing financial interests or personal relationships that could have appeared to influence the work reported in this paper.

Data availability

No data was used for the research described in the article.

Acknowledgements

This research is supported by Open Project fund of Key Laboratory of High-efficiency and Clean Mechanical Manufacture (Shandong University), Ministry of Education.

References

[1] S. Petersen, et al., News from the seabed – geological characteristics and resource potential of deep-sea mineral resources, Mar. Pol. 70 (2016) 175–187.
[2] N.E. Leonard, D.A. Paley, F. Lekien, R. Sepulchre, D.M. Fratantoni, R.E. Davis, Collective motion, sensor networks, and ocean sampling, Proc. IEEE 95 (1) (Jan. 2007) 48–74.
[3] News from the Seabed–Geological Characteristics and Resource Potential of Deep-Sea Mineral Resources Mar Policy, vol. 70, 2016, pp. 175–187.
[4] M. Belbeoch, Argo-Part of the Integrated Global Observation Strategy, Dec. 2012 ([Online]).
[5] J. Sherman, R.E. Davis, W.B. Owens, J. Valdes, The autonomous underwater glider "Spray, IEEE J. Ocean. Eng. 26 (4) (Oct. 2001) 437–446.
[6] D.C. Webb, P.J. Simonetti, C.P. Jones, SLOCUM: an underwater glider propelled by environmental energy, IEEE J. Ocean. Eng. 26 (4) (Oct. 2001) 447–452.
[7] G. Wang, Y. Yang, S. Wang, Ocean thermal energy application technologies for unmanned underwater vehicles: a comprehensive review, Appl. Energy 278 (2020), 115752.
[8] H. Stommel, The slocum mission, Oceanography 2 (1) (1989) 22–25, https://doi.org/10.5670/oceanog.1989.26.
[9] M. Klein Altstedde, F. Rinderknecht, H. Friedrich, Integrating phase-change materials into automotive thermoelectric generators, J. Electron. Mater. 43 (2014) 2134–2140.
[10] J. Jones, Y. Chao, Utilizing Ocean Thermal Energy in a Submarine Robot, vol. 2009, NASA Tech Briefs, January, 2009.
[11] D. C. Webb, P. J. Simonetti and C. P. Jones, "SLOCUM: an underwater glider propelled by environmental energy," in IEEE J. Ocean. Eng., vol. 26, no. 4, pp. 447-452.
[12] NASA demonstrates novel ocean-powered underwater vehicle[EB/OL]. https://www.nasa.gov/centers/jpl/news/earth2010.0405.html.
[13] Tauseef-ur-Rehman, et al., A critical review on heat transfer augmentation of phase change materials embedded with porous materials/foams, Int. J. Heat Mass Tran. 135 (2019) 649–673.
[14] J.F. Li, et al., Simultaneous enhancement of latent heat and thermal conductivity of docosane-based phase change material in the presence of spongy graphene, Sol. Energy Mater. Sol. Cell. 128 (2014) 48–51.
[15] R. Kalbasi, M.R. Salimpour, Constructal design of horizontal fins to improve the performance of phase change material rectangular enclosures, Appl. Therm. Eng. 91 (2015) 234–244.
[16] B. Rajabifar, et al., Flow and Heat Transfer in Micro Pin Fin Heat Sinks with Nano-Encapsulated Phase Change Materials, 2016.
[17] A.M. Abdulateef, et al., Geometric and design parameters of fins employed for enhancing thermal energy storage systems: a review, Renew. Sustain. Energy Rev. 82 (2018) 1620–1635.
[18] N.H.S. Tay, F. Bruno, M. Belusko, Comparison of pinned and finned tubes in a phase change thermal energy storage system using CFD, Appl. Energy 104 (2013) 79–86.
[19] J. Duan, Y. Xiong, D. Yang, Study on the effect of multiple spiral fins for improved phase change process, Appl. Therm. Eng. 169 (2020), 114966.
[20] A. Rozenfeld, et al., Experimental demonstration, modeling and analysis of a novel latent-heat thermal energy storage unit with a helical fin, Int. J. Heat Mass Tran. 110 (2017) 692–709.
[21] A.A. Al-Abidi, et al., Numerical study of PCM solidification in a triplex tube heat exchanger with internal and external fins, Int. J. Heat Mass Tran. 61 (2013) 684–695.
[22] A.A. Al-Abidi, et al., Experimental study of melting and solidification of PCM in a triplex tube heat exchanger with fins, Energy Build. 68 (2014) 33–41.
[23] M.J. Hosseini, et al., Experimental and numerical evaluation of longitudinally finned latent heat thermal storage systems, Energy Build. 99 (2015) 263–272.
[24] M. Zhao, et al., Topology optimization of fins for energy storage tank with phase change material, Numer. Heat Tran. Part A, Applications 77 (3) (2020) 284–301.
[25] A. Sciacovelli, F. Gagliardi, V. Verda, Maximization of performance of a PCM latent heat storage system with innovative fins, Appl. Energy 137 (2015) 707–715.
[26] C. Zhang, J. Li, Y. Chen, Improving the energy discharging performance of a latent heat storage (LHS) unit using fractal-tree-shaped fins, Appl. Energy 259 (2020), 114102.
[27] Bingzhen Wang, Ge Wang, Wei Zhang, Design and experimental of heat transfer system for small-scale temperature difference energy generation device, J. Mar. Technol. 36 (4) (2017) 47–52.
[28] K.A.R. Ismail, C.L.F. Alves, M.S. Modesto, Numerical and experimental study on the solidification of PCM around a vertical axially finned isothermal cylinder, Appl. Therm. Eng. 21 (Issue 1) (2001) 53–77.
[29] Q. Xia, et al., A new model of phase change process for thermal energy storage, Int. J. Energy Res. 42 (12) (2018) 3877–3887.